



# A Multivariate Diagnostic Model Based on Urinary EpCAM-CD9-Positive Extracellular Vesicles for Prostate Cancer Diagnosis

Yibei Dai<sup>1†</sup>, Yiyun Wang<sup>2†</sup>, Ying Cao<sup>1</sup>, Pan Yu<sup>1</sup>, Lingyu Zhang<sup>1</sup>, Zhenping Liu<sup>3</sup>, Ying Ping<sup>1</sup>, Danhua Wang<sup>1</sup>, Gong Zhang<sup>1</sup>, Yiwen Sang<sup>1</sup>, Xuchu Wang<sup>1\*</sup> and Zhihua Tao<sup>1\*</sup>

<sup>1</sup> Department of Laboratory Medicine, The Second Affiliated Hospital of Zhejiang University School of Medicine, Hangzhou, China, <sup>2</sup> Zhejiang University School of Medicine, Hangzhou, China, <sup>3</sup> Department of Laboratory Medicine, The First People's Hospital of Yuhang District, Hangzhou, China

## OPEN ACCESS

### Edited by:

Antonina Mitrofanova,  
Rutgers, The State University of New  
Jersey, United States

### Reviewed by:

Bilal A. Siddiqui,  
University of Texas MD Anderson  
Cancer Center, United States  
Mariana Chantre Justino,  
Rio de Janeiro State University, Brazil

### \*Correspondence:

Zhihua Tao  
rtzh@zju.edu.cn  
Xuchu Wang  
wangxc@zju.edu.cn

<sup>†</sup>These authors have contributed  
equally to this work

### Specialty section:

This article was submitted to  
Genitourinary Oncology,  
a section of the journal  
Frontiers in Oncology

**Received:** 15 September 2021

**Accepted:** 29 October 2021

**Published:** 24 November 2021

### Citation:

Dai Y, Wang Y, Cao Y, Yu P,  
Zhang L, Liu Z, Ping Y, Wang D,  
Zhang G, Sang Y, Wang X and  
Tao Z (2021) A Multivariate Diagnostic  
Model Based on Urinary EpCAM-  
CD9-Positive Extracellular Vesicles  
for Prostate Cancer Diagnosis.  
*Front. Oncol.* 11:777684.  
doi: 10.3389/fonc.2021.777684

**Introduction:** Prostate cancer (PCa) is one of the most frequently diagnosed cancers and the leading cause of cancer death in males worldwide. Although prostate-specific antigen (PSA) screening has considerably improved the detection of PCa, it has also led to a dramatic increase in overdiagnosing indolent disease due to its low specificity. This study aimed to develop and validate a multivariate diagnostic model based on the urinary epithelial cell adhesion molecule (EpCAM)-CD9-positive extracellular vesicles (EVs) (uEV<sub>EpCAM-CD9</sub>) to improve the diagnosis of PCa.

**Methods:** We investigated the performance of uEV<sub>EpCAM-CD9</sub> from urine samples of 193 participants (112 PCa patients, 55 benign prostatic hyperplasia patients, and 26 healthy donors) to diagnose PCa using our laboratory-developed chemiluminescent immunoassay. We applied machine learning to training sets and subsequently evaluated the multivariate diagnostic model based on uEV<sub>EpCAM-CD9</sub> in validation sets.

**Results:** Results showed that uEV<sub>EpCAM-CD9</sub> was able to distinguish PCa from controls, and a significant decrease of uEV<sub>EpCAM-CD9</sub> was observed after prostatectomy. We further used a training set (N = 116) and constructed an exclusive multivariate diagnostic model based on uEV<sub>EpCAM-CD9</sub>, PSA, and other clinical parameters, which showed an enhanced diagnostic sensitivity and specificity and performed excellently to diagnose PCa [area under the curve (AUC) = 0.952, P < 0.0001]. When applied to a validation test (N = 77), the model achieved an AUC of 0.947 (P < 0.0001). Moreover, this diagnostic model also exhibited a superior diagnostic performance (AUC = 0.917, P < 0.0001) over PSA (AUC = 0.712, P = 0.0018) at the PSA gray zone.

**Conclusions:** The multivariate model based on uEV<sub>EpCAM-CD9</sub> achieved a notable diagnostic performance to diagnose PCa. In the future, this model may potentially be used to better select patients for prostate transrectal ultrasound (TRUS) biopsy.

**Keywords:** extracellular vesicle, EpCAM, chemiluminescent immunoassay, prostate cancer, multivariate diagnostic model

## INTRODUCTION

Prostate cancer (PCa) is one of the most frequently diagnosed cancers and the leading cause of cancer death in males worldwide (1). Despite the widespread use of prostate-specific antigen (PSA) as a noninvasive screening tool for PCa, the low specificity of PSA has led to an increase in either overdiagnosis or unnecessary biopsies, especially when its value is within the PSA gray zone (4–10 ng/ml) (2, 3). Thus, it is urgently needed to explore new biomarkers for more accurate PCa diagnosis.

Urine is an ideal source of PCa biomarkers because the samples can be collected noninvasively in large amounts, and several urinary markers have been reported such as prostate cancer antigen-3 (PCA3), transmembrane protease serine-2 (TMPRSS2), and glutathione S-transferase P (GSTP1) gene (4–7). Recently, urinary extracellular vesicles (uEVs) have sparked interest as potential biomarkers (8, 9). uEVs are low-density membrane vesicles containing lipids, proteins, DNA, mRNAs, and microRNAs (10). A reproducible method for uEV isolation has been described by Pisitkun et al. (11) in 2004 and has been widely adopted for uEV analysis. Previous proteomic analysis of uEVs has revealed varieties of cancer-specific proteins in their cargoes (12, 13). However, the question remained whether there is a specific protein in uEVs that could provide diagnostic information for PCa and also be easily detected.

Epithelial cell adhesion molecule (EpCAM) is a transmembrane glycoprotein that plays an important role in Ca<sup>2+</sup>-independent hemophilic cell-to-cell adhesion, cell signaling, migration, proliferation, and differentiation of cancer cells (14, 15). It has thus gained considerable attraction as an appealing candidate biomarker for cancer diagnosis due to its strong expression in various carcinomas and their metastases compared with normal epithelia (16, 17). Recently, EpCAM on tumor-derived EV membrane was also employed as a promising tumor surface marker, while the tetraspanin family of proteins, such as CD63, CD9, and CD81, was mainly used as EV universal markers (18, 19). The use of these biomarkers to identify EVs

from bodily fluids has garnered much interest as a non-invasive liquid biopsy for cancer.

Accordingly, we herein aimed to develop and validate a multivariate diagnostic model based on the urinary EpCAM-CD9-positive EVs (uEV<sub>EpCAM-CD9</sub>) to improve the diagnosis of PCa. We first investigated the performance of uEV<sub>EpCAM-CD9</sub> for the diagnosis of PCa using a newly laboratory-developed chemiluminescent immunoassay (CLIA) (**Figure 1A**). Briefly, uEV<sub>EpCAM-CD9</sub> diffused in urine is bound with acridinium ester (ACE)-labeled anti-CD9 antibodies and captured by magnetic bead-labeled anti-EpCAM antibodies, followed by a thorough isolation under an external magnetic field. Consequently, the concentrations of EpCAM-CD9-positive EVs (EV<sub>EpCAM-CD9</sub>) can be quantitatively determined by measuring the chemiluminescent signals. Results indicated that EV<sub>EpCAM-CD9</sub> from the culture supernatant of PCa cell lines were significantly elevated under the simulated tumor microenvironment. Moreover, preliminary results showed that uEV<sub>EpCAM-CD9</sub> could distinguish patients with PCa from control sets, indicating that uEV<sub>EpCAM-CD9</sub> may be a potential biomarker for PCa diagnosis. We then applied machine learning to training sets and subsequently evaluated the multivariate diagnostic model based on uEV<sub>EpCAM-CD9</sub> in validation sets.

## MATERIALS AND METHODS

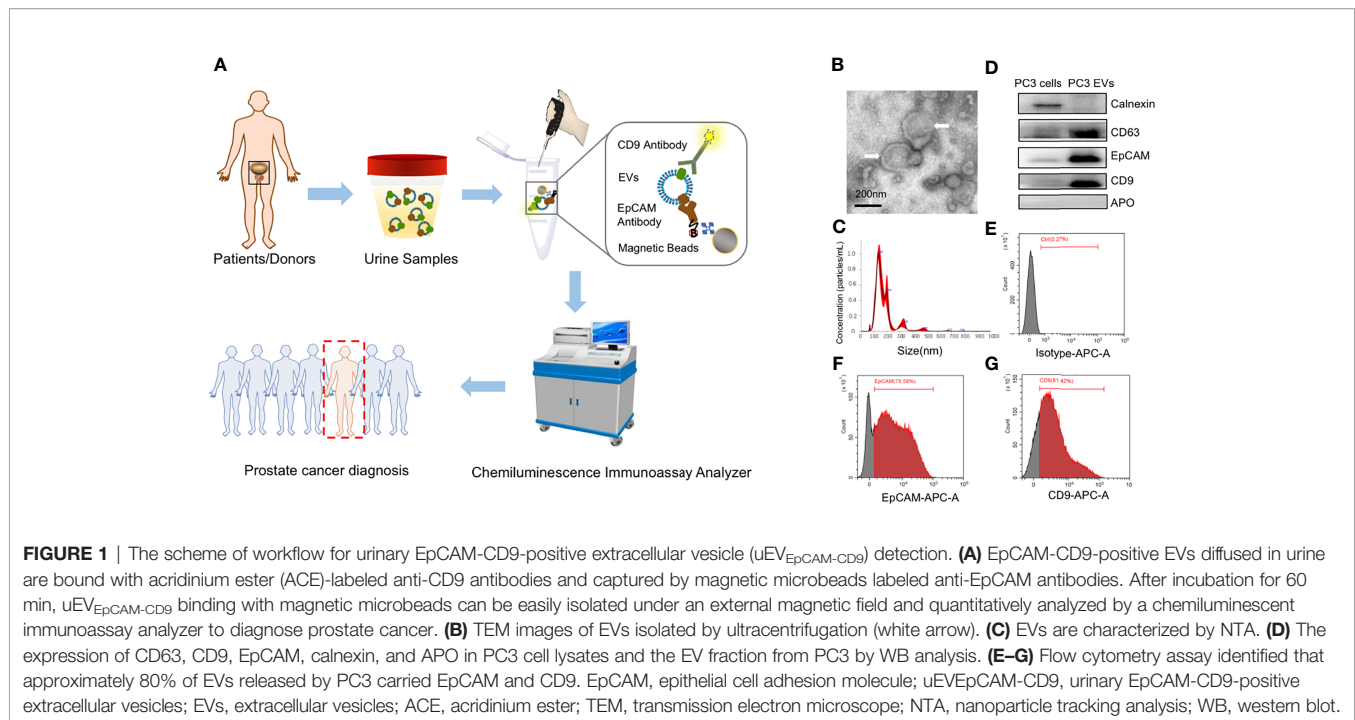
### Cell Lines and Culture

Two human PCa cell lines (PC3 and LNCaP) and an immortalized prostate epithelial cell line (RWPE-1) were obtained from the American Type Culture Collection (Manassas, VA, USA). All cell lines were cultured in RPMI 1640 medium (Gibco Invitrogen, Carlsbad, CA, USA) supplemented with 10% fetal bovine serum (FBS; Thermo Fisher Scientific, MA, USA), 100 U/ml penicillin, and 100 µg/ml streptomycin in an incubator with 5% CO<sub>2</sub> at 37°C.

### Urine Collection

Urine samples from 193 participants [112 PCa patients, 55 benign prostatic hyperplasia (BPH) patients, and 26 healthy donors (HDs)] were collected in the Second Affiliated Hospital of Zhejiang University School of Medicine. Approval was obtained from the Second Affiliated Hospital of Zhejiang University School of Medicine Ethical Committee before initiating the study. Detailed information on the patients is summarized in **Supplementary Table S1**. All methods were performed in accordance with the relevant guidelines and regulations. All the patients met the following inclusion criteria: (1) undergoing prostate biopsy for the first time, (2) three-dimensional size of the prostate available *via* transabdominal ultrasonography before biopsy, (3) blood tests performed within 1 week before biopsy, (4) complete clinical and pathological data available, (5) absence of acute prostatitis or systemic inflammatory disease, (6) absence of urinary tract infection, (7) no history of prostate surgery, (8) no history of

**Abbreviations:** EpCAM, epithelial cell adhesion molecule; PCa, prostate cancer; PSA, prostate-specific antigen; EVs, extracellular vesicles; uEV<sub>EpCAM-CD9</sub>, urinary EpCAM-CD9-positive extracellular vesicles; AUC, area under the curve; TRUS, transrectal ultrasound; PCA3, prostate cancer antigen-3; TMPRSS2, transmembrane protease serine-2; GSTP1, glutathione S-transferase; uEVs, urinary extracellular vesicles; CLIA, chemiluminescent immunoassay; ACE, acridinium ester; EV<sub>EpCAM-CD9</sub>, EpCAM-CD9-positive extracellular vesicles; FBS, fetal bovine serum; BPH, benign prostatic hyperplasia; HD, healthy donor; PBS, phosphate-buffered saline; TEM, transmission electron microscope; NTA, nanoparticle tracking analysis; RIPA, radioimmunoprecipitation assay; SDS-PAGE, sodium dodecyl sulfate-polyacrylamide gel electrophoresis; PVDF, polyvinylidene difluoride; TBST, Tris-buffered saline with Tween-20; WB, western blot; HRP, horseradish peroxidase; Density<sub>EpCAM-CD9</sub>, EpCAM-CD9 protein density; BCA, bicinchoninic acid; SD, standard deviation; IQR, interquartile range; ROC, receiver operating characteristic; DCA, decision curve analysis; RCU, relative chemiluminescent unit; LOD, limit of detection; intra-CV, intra-assay coefficient of variation; inter-CV, inter-assay coefficient of variation; CI, confidence interval; OR, odds ratio; fPSA, free prostate-specific antigen; f/t PSA, free/total prostate-specific antigen; PV, prostate volume; PSAD, prostate-specific antigen density; BMI, body mass index; EMT, epithelial–mesenchymal transition; CRPC, castration-resistant prostate cancer.



5-alpha reductase inhibitor use, and (9) no anti-inflammatory drug use within 2 weeks before blood tests. Initial voided urine (5–10 ml) was prospectively collected from patients at the time of day most convenient to the person before prostate biopsy. Matched urine samples were collected from PCa patients prior to ( $n = 10$ ) and a week after local treatment by radical prostatectomy ( $n = 10$ ).

## Extracellular Vesicle Isolation From Cell Culture Medium and Urine

EVs were isolated from cell culture medium by ultracentrifugation as previously described (20). Briefly, when 70%–80% confluency was reached, cells were washed twice with phosphate-buffered saline (PBS; pH7.0) and then incubated for 48 h in FBS-free medium. Cell culture medium was collected and subjected to consecutive centrifugation steps ( $300 \times g$  for 10 min and  $2,000 \times g$  for 20 min) to remove dead cells and cellular debris. The supernatant was vacuum filtered using a 10-kDa centrifugal filter (Merck Millipore, Darmstadt, Germany), and EV concentrates were ultracentrifuged at  $100,000 \times g$  for 70 min at  $4^\circ\text{C}$  (Type 70 Ti Fixed-angle Titanium Rotor,  $k$  factor = 157.4) (Optima<sup>TM</sup> XP ultracentrifuge; Beckman Coulter, Indianapolis, IN, USA). Pellets were washed with PBS followed by ultracentrifugation at the same speed and time. The supernatant was discarded, and the resulting EV pellets were suspended in PBS and stored at  $-80^\circ\text{C}$ .

In order to obtain uEVs, urine samples from patients with PCa, BPH and HDs were centrifuged at  $3,000 \times g$  for 20 min at  $4^\circ\text{C}$  to remove debris and then ultracentrifuged at  $200,000 \times g$  for 2 h at  $4^\circ\text{C}$ . The supernatant was removed, and the uEV pellets were resuspended in PBS and stored at  $-80^\circ\text{C}$ .

## Transmission Electron Microscopy

Transmission electron microscope (TEM) was used to investigate the morphology of the EVs isolated by ultracentrifugation. Briefly, EVs at an optimal concentration were first placed on 400 mesh carbon/formvar-coated grids and allowed to be absorbed on formvar for a minimum of 10 min. Next, the grids (membrane side down) were transferred to a 50- $\mu\text{l}$  drop of 2.5% glutaraldehyde for 5 min, after which they were transferred to a 100- $\mu\text{l}$  drop of distilled water and were left to stand for 2 min. This process was repeated nine times for a total of 10 water washes. Then, the sample was loaded on the grid and stained by 4% uranyl acetate for 10 min and 1% methylcellulose for 5 min. The remaining water was removed using filter paper. Finally, the samples were viewed using a Tecnai Bio Twin TEM (FEI, Hillsboro, OR, USA), and images were obtained using an AMT CCD camera (Advanced Microscopy Techniques, Woburn, MA, USA).

## Nanoparticle Tracking Analysis

The concentration and the size distribution of EVs were analyzed by nanoparticle tracking analysis (NTA) using a ZetaView instrument (Particle Metrix, Inning am Ammersee, Germany) and the NanoSight LM10 microscope (NanoSight Ltd., Amesbury, UK) configured with a 405-nm laser. Videos were collected and analyzed using the NTA software (version 2.3) with the default setting of the minimal expected particle size, minimum track length, and blur. Each EV sample was vortexed and diluted with particle-free PBS to obtain the recommended 25–100 particles/frame of the NTA system. Five videos of typically 60-s duration were recorded to generate replicate histograms that were averaged.

## Western Blot Analysis

Cells and EVs were lysed in radioimmunoprecipitation assay (RIPA) Lysis Buffer (Beyotime Biotechnology, Shanghai, China) for 30 min on ice, and the protein concentration was measured by the Enhanced BCA Protein Assay Kit (Beyotime Biotechnology, Shanghai, China). And then, the lysates were mixed with loading buffer and heated to 100°C for 10 min. Subsequently, the samples were electrophoretically separated on an 8% sodium dodecyl sulfate–polyacrylamide gel electrophoresis (SDS-PAGE) and electro-transferred onto polyvinylidene difluoride (PVDF) membranes (Millipore, Carlsbad, CA). After blocking for 2 h at 25°C in Tris-buffered saline with 0.05% Tween-20 (TBST) and 5% non-fat dry milk, the membranes were incubated overnight at 4°C with the primary antibodies in TBST containing 5% BSA. The following antibodies were used for Western blot (WB) analysis, including anti-Alix antibody (1:1,000; ab88388; Abcam, Cambridge, MA, USA), anti-Calnexin antibody (1:200; ab238078; Abcam, Cambridge, MA, USA), anti-CD63 antibody (1:300; ab8219; Abcam, Cambridge, MA, USA), anti-EpCAM antibody (1:200; ab218448; Abcam, Cambridge, MA, USA), anti-CD9 antibody (1:300; sc-13118; Santa-Cruz Biotechnology, Santa Cruz, CA, USA), anti-beta Actin antibody (1:5,000; ab6276; Abcam, Cambridge, MA, USA), and anti-Apo antibody (1:500; ab66379; Abcam, Cambridge, MA, USA). Thereafter, the membrane was washed and immersed into horseradish peroxidase (HRP)-conjugated secondary antibodies (Jackson ImmunoResearch, Suffolk, UK) for 2 h at 25°C. Chemiluminescent detection of bands was performed using Clarity Western ECL Substrate Kit (Bio-Rad Laboratories, Inc., Hercules, CA, USA), and the signals were visualized using the Quantity One Imaging Software from Bio-Rad according to the manufacturer's instructions. In order to quantify the levels of EpCAM-CD9-positive EVs from WB analysis and investigate the association with the chemiluminescent signals by our immunoassay, we rationally defined the EpCAM-CD9 protein density ( $Density_{EpCAM-CD9}$ ):  $Density_{EpCAM-CD9} = Density_{EpCAM} \times Density_{CD9}$ , where the value of  $Density_{EpCAM}$  and  $Density_{CD9}$  can be quantitatively obtained from WB images using Quantity One Imaging Software. This definition was based on the hypothesis that all the EVs expressing EpCAM and CD9 were sufficiently captured and detected by the antibody sets of our immunoassay, and the chemiluminescent signals of each EV captured by EpCAM antibody can be multiplied by CD9 antibody. Our results showed that  $Density_{EpCAM-CD9}$  was correlated highly with chemiluminescent signals ( $r = 0.8395$ , 95% CI: 0.6317–0.9348,  $P < 0.0001$ ) (Supplementary Figure S2A).

## Flow Cytometry Analysis

The expression of CD9 and EpCAM on EVs were analyzed by flow cytometry as previously described (21). Briefly, EVs attached to 4  $\mu$ m aldehyde/sulfate latex beads (Invitrogen, Carlsbad, CA, USA) were incubated with anti-CD9 antibodies (SAB4700092; Sigma-Aldrich, St. Louis, MO), anti-CD63 antibodies (ab1318; Abcam, Cambridge, MA, USA), anti-CD81 antibodies (ab79559; Abcam, Cambridge, MA, USA), or anti-

EpCAM antibodies (ab187372; Abcam, Cambridge, MA, USA) for 30 min with rotation at 4°C followed by Alexa-488-tagged secondary antibodies (Life Technologies, Carlsbad, CA, USA) for 30 min with rotation at 4°C. Samples were detected using CytoFLEX Flow Cytometer (Beckman Coulter, Brea, CA, USA) and data were analyzed using CytExpert (Beckman Coulter, Brea, CA, USA).

## Bicinchoninic Acid Assay

According to the manufacturer's instructions, the concentration and the protein amount of EVs were measured by bicinchoninic acid (BCA) assay using Enhanced BCA Protein Assay Kit (Beyotime Biotechnology, Shanghai, China) and a spectrophotometer (Bio-Rad Laboratories, Inc., Hercules, CA, USA) set to 562 nm.

## Urinary Creatinine and Serum Prostate-Specific Antigen

The urinary creatinine was measured with Roche-developed assays for creatinine (CRE2U, ACN 8152) using a Roche Cobas 8000 Modular Analyzer (Roche, Woerden, Netherlands) according to the manufacturer's instructions. The automated chemiluminescent microparticle immunoassay analyzer ARCHITECT i2000 (Abbott Laboratories, Abbott Park, IL, USA) was used following the manufacturer's protocols to determine the concentrations of PSA protein in serum samples.

## Serum Starvation and Hypoxia for Cells

Cells were seeded and cultured in RPMI 1640 medium, which contains glucose and amino acids for 24 h. The medium was discarded, and then cells were washed once with PBS to remove trace serum. The cells were further cultured in serum-free RPMI 1640 medium under normoxia (21% O<sub>2</sub>) to suffer serum starvation or cultured in RPMI 1640 medium supplemented with 10% FBS under hypoxic conditions (1% O<sub>2</sub>) to suffer hypoxia for the indicated time periods.

## Chemiluminescent Immunoassay for Extracellular Vesicle Detection

EVs were detected by a newly developed paramagnetic particle-based sandwich CLIA (Figure 1A).

For EVs from the cell line supernatant, 100  $\mu$ l EVs were mixed with 50  $\mu$ l ACE-labeled anti-CD9 antibodies (1.320  $\mu$ g/ml) and biotin-labeled anti-EpCAM antibodies (4.000  $\mu$ g/ml). After incubation for 1 h at 25°C, the mixtures are incubated with 50  $\mu$ l turbid liquid containing 4 mg/ml avidin-coated magnetic beads for another 30 min, followed by thorough washing of the magnetic beads under an external magnetic field. Finally, magnetic beads with ACE-labeled anti-CD9 antibodies are mixed with trigger solution for chemiluminescent signal excitation. All the measurements are performed in triplicate.  $EV_{EpCAM-CD9}$  secretion index was calculated to describe the average amount of  $EV_{EpCAM-CD9}$  secreted per PC3 cell.  $EV_{EpCAM-CD9}$  secretion index =  $V_s \times Con_{EV} / N_{cell}$ , where  $V_s$  ( $\mu$ l) is the volume of the PC3 cell line supernatant,  $Con_{EV}$  (particles/ $\mu$ l) is the concentration of  $EV_{EpCAM-CD9}$  derived by

PC3 cells in the supernatant, and  $N_{\text{cell}}$  corresponds to the number of the PC3 cells.

For EVs from the urine samples, each step was the same as the EVs from the cell line supernatant, except the concentration of the ACE-labeled anti-CD9 antibodies (0.132  $\mu\text{g/ml}$ ). To avoid urine sampling variance,  $uEV_{\text{EpCAM-CD9}}$  concentrations were normalized by urinary creatinine. We herein rationally defined “n.u.”: n.u. =  $\text{Con EV}/\text{Cr}$ , where Con EV (g/L) corresponds to the concentration of  $EV_{\text{EpCAM-CD9}}$  in the urine samples and Cr (g/L) corresponds to the urinary creatinine of the urine samples, to compare  $uEV_{\text{EpCAM-CD9}}$  concentrations between patients with PCa and without PCa better.

## Statistical Analysis

Continuous variables were presented as mean  $\pm$  standard deviation (SD) or median [interquartile range (IQR)] and compared with each other by Student's t-test or Mann-Whitney U test. Categorical variables are presented as rate and compared using the chi-square test or the Fisher's exact test. Receiver operating characteristic (ROC) curve was used to evaluate the diagnostic performance of EpCAM-CD9-positive EVs, PSA, and models. Decision curve analysis (DCA) was used to compare the diagnostic benefits of different biomarkers and models for PCa. P-values lower than 0.05 were considered statistically significant. All analyses were undertaken with GraphPad Prism version 8.0, SPSS Statistics 20, and R version 2.10.1 (R Foundation for Statistical Computing; <http://www.R-project.org>).

## RESULTS

### Characterization of Extracellular Vesicles From the Prostate Cell Line PC3

In this study, we used PC3-derived EVs to construct and optimize the CLIA. Standard characterization of EVs was performed using TEM, NTA, and WB analysis (**Figures 1B–D**). EVs showed characteristic cup-shaped morphology under TEM and showed a mean size of  $175.9 \pm 6.3$  nm (standard error; SD:  $78.6 \pm 11.1$  nm) by NTA. The EV fraction from PC3 was enriched in CD63, CD9, and ALIX, the common biomarkers of EVs, but did not contain calnexin and APO, the negative control of EVs, compared to the PC3 cell lysates (20). In addition, PC3-derived EVs were positive for EpCAM, an epithelial cell marker. Moreover, flow cytometry assay identified that approximately 80% of EVs released by PC3 carried EpCAM and CD9 (**Figures 1E–G**). These results indicated that EpCAM and CD9 were enriched on the membrane of EVs from the prostate cell line PC3 and EVs can be effectively captured by anti-EpCAM antibody-conjugated magnetic beads and successfully detected by ACE-labeled anti-CD9 antibodies.

### Ultrasensitive Detection of EpCAM-CD9-Positive Extracellular Vesicles by Chemiluminescent Immunoassay

We performed an ultrasensitive CLIA to quantify  $EV_{\text{EpCAM-CD9}}$  (**Figure 1A**). Noteworthy, although several conventional surface

markers (e.g., CD9, CD63, and CD81) are used for EV analysis, we selected CD9 as our detection antibody for EVs. The expression of CD9, CD63, CD81, and EpCAM on PC3-derived EVs were analyzed by flow cytometry in our study, showing that EVs carrying CD9, CD63, CD81, and EpCAM accounted for 81.42%, 82.08%, 67.19%, and 79.59% of total PC3-derived EVs, respectively. Practically, the CLIA employing ACE-labeled anti-CD9 antibody exhibited a superior performance over ACE-labeled CD63 antibody or ACE-labeled CD81 antibody (data not shown). This assay exhibited remarkable chemiluminescent signals for PC3-derived EVs, while the four control groups (non-EVs, non-streptavidin-labeled magnetic beads, non-biotin-labeled anti-EpCAM antibodies, and non-ACE-labeled anti-CD9 antibodies) presented negligible chemiluminescent signals (**Figure 2A**). By contrast, a significant reduction in the relative chemiluminescent unit (RCU) was observed after the addition of Triton X-100, a detergent to lyse EVs (**Figure 2B**) (22). These results strongly demonstrated the feasibility of the assay for selectively detecting EVs.

Next, we systematically optimized the reaction conditions of the EV assay, including the concentration of streptavidin-labeled magnetic beads, biotin-labeled anti-EpCAM antibodies, ACE-labeled anti-CD9 antibodies, and reaction time (**Supplementary Figures S1A–D**). To further investigate the quantitative performance of the EV assay, isolated PC3-derived EVs by ultracentrifugation were quantified using the EV assay based on the concentrations obtained by NTA. As shown in **Figure 2C**, the RCU value was found to greatly depend on the concentration of EVs, with a good linearity range ranging from  $5.50 \times 10^4$  to  $8.80 \times 10^5$  particles/ $\mu\text{l}$  ( $R^2 = 0.9823$ ). The limit of detection (LOD) calculated as three times of SD above the background (negative control) was  $2.86 \times 10^4$  particles/ $\mu\text{l}$ . Moreover, PC3-derived EVs were quantified by a standard procedure of a recovery test to evaluate the accuracy of the EV assay. The recovery rates of low, medium, and high concentrations of EVs were 85.45%, 95.45%, and 101.65%, respectively (**Supplementary Table S2**, left panels). In addition, three different concentrations of EVs were tested to evaluate the repeatability of the EV assay. The intra-assay coefficient of variation (intra-CV) and the inter-assay coefficient of variation (inter-CV) were less than 10% and 20%, respectively (**Supplementary Table S2**, left panels). The above results suggested an excellent analytical performance of our EV assay.

Then, we asked whether the  $EV_{\text{EpCAM-CD9}}$  could be used to infer the prostatic cell types, e.g., PCa cell lines (PC3 and LNCaP) and benign prostate epithelial cell line (RWPE-1). Hence, we obtained the EVs from the culture supernatant by ultracentrifugation and quantified the concentrations by our assay. As shown in **Figure 2D**, the concentrations of EVs derived from human PCa cell lines such as PC3 and LNCaP were significantly higher than that of the BPH cell line RWPE-1, which were consistent with the  $EV_{\text{Density}_{\text{EpCAM-CD9}}}$  from corresponding cell lines. Moreover, FBS-derived EVs exhibited negligible chemiluminescent signals in the assay. These results revealed that the concentration of  $EV_{\text{EpCAM-CD9}}$  can be a potential indicator for distinguishing cancerous cells from normal ones.

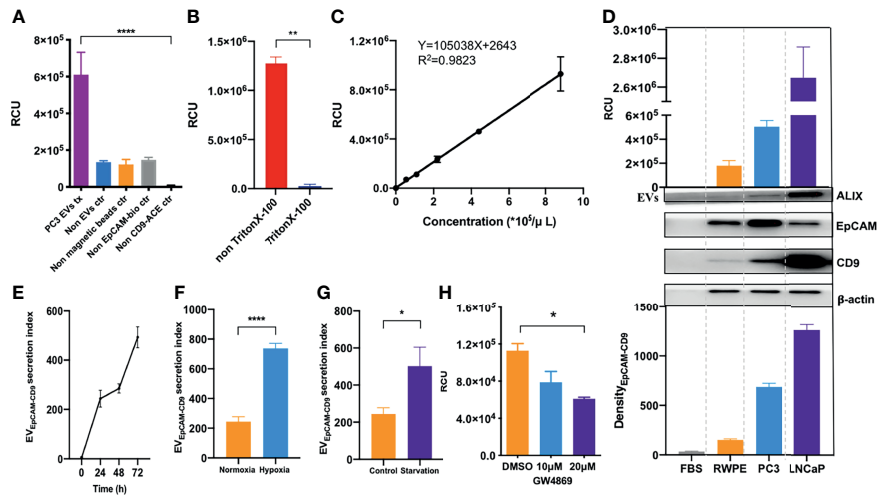


**FIGURE 2** |  $EV_{EpCAM-CD9}$  is ultrasensitively detected by chemiluminescent immunoassay and oversecreted under simulated tumor microenvironment. **(A)** Groups of PC3 EVs, non-EVs, non-streptavidin-labeled magnetic beads, non-biotin-labeled anti-EpCAM antibodies, and non-ACE-labeled anti-CD9 antibodies were detected by our assay. **(B)** EVs were penetrated by Triton X-100. **(C)** A standard curve was for EVs from cell line supernatant quantification using our EV assay. **(D)** EVs derived from FBS, BPH cell line RWPE-1, and human prostate cancer cell lines PC3 and LNCaP were detected by our EV assay and WB. **(E)** The changes of  $EV_{EpCAM-CD9}$  secretion index during the growth of PC3 cells. **(F)** The changes of  $EV_{EpCAM-CD9}$  secretion index when the PC3 cells were cultured under hypoxia. **(G)** The changes of  $EV_{EpCAM-CD9}$  secretion index when the PC3 cells were cultured under serum starvation. **(H)** The changes of  $EV_{EpCAM-CD9}$  secreted by PC3 cells with the treatment of 10 and 20  $\mu$ M GW4869. RCU, relative chemiluminescent unit; EVs, extracellular vesicles; FBS, fetal bovine serum;  $EV_{EpCAM-CD9}$ , EpCAM-CD9-positive extracellular vesicles. \* $P < 0.05$ , \*\* $P < 0.01$ , \*\*\*\* $P < 0.0001$ .

## $EV_{EpCAM-CD9}$ Are Oversecreted by Prostate Cancer Cells Under Simulated Tumor Microenvironment

In the course of tumor expansion, cancer cells within the tumor microenvironment often have restricted access to nutrients and oxygen and thus were subjected to starvation and hypoxia (23). Previous reports have demonstrated that the levels of EVs carrying tumor-related proteins can be significantly elevated under such microenvironment, contributing to the regulation of tumor microenvironment, thus promoting tumor initiation, progression, and metastasis (24). However,  $EV_{EpCAM-CD9}$  derived from PCa cells under tumor microenvironment, which may be diagnostically beneficial in reflecting the pathological stage during PCa development, remained unknown.

Herein, we defined  $EV_{EpCAM-CD9}$  secretion index to describe the average amount of  $EV_{EpCAM-CD9}$  secreted per PC3 cell. As shown in **Figure 2E**, the  $EV_{EpCAM-CD9}$  secretion index was gradually elevated at the early stage of cell growth due to the initial activation of the cells in the latent phase. At 24–48 h, the PC3 cells entered the logarithmic growth phase, and the equative rate of increase between the amount of  $EV_{EpCAM-CD9}$  and PC3 cells resulted in a constant  $EV_{EpCAM-CD9}$  secretion index. Interestingly, however, when the cell reached the stationary phase after 48 h, the  $EV_{EpCAM-CD9}$  secretion index started increasing again. This may be a result of the inadequate living conditions in the microenvironment. Accordingly, we investigated the impact of some conditions (e.g., hypoxia and serum starvation) involved in such microenvironment on the

$EV_{EpCAM-CD9}$  secretion index. We observed higher  $EV_{EpCAM-CD9}$  secretion indexes when the PC3 cells were cultured under hypoxia and serum starvation compared with the controls (**Figures 2F, G**). Additionally, this trend can be reversed upon the treatment of the EV biogenesis inhibitor, such as GW4869 (**Figure 2H**). These results strongly support our hypothesis that  $EV_{EpCAM-CD9}$  can be a potential indicator in revealing the pathological status of PCa.

## Urinary EpCAM-CD9-Positive Extracellular Vesicle Is a Biomarker for Prostate Cancer Diagnosis

Urine can harbor PCa cell-derived EVs, as mentioned above. We thus investigated whether the urinary EpCAM-CD9-positive EVs ( $uEV_{EpCAM-CD9}$ ) can be detected using our EV assay. As shown in **Supplementary Figure S2B**, the protein profile from urine revealed the presence of EpCAM and CD9-positive EVs in PCa. Using a well-adopted EV protein assay, WB,  $uEV_{EpCAM-CD9}$  from less than 2 ml of urine volume was almost undetectable (**Figure 3A**). However, the  $uEV_{EpCAM-CD9}$  from even down to 125  $\mu$ l of urine volume could be successfully detected by our CLIA, and the levels of  $uEV_{EpCAM-CD9}$  in the same urine volume were statistically distinguishable between the pooled samples from PCa and healthy controls (**Figures 3B, C**). In view of the significant differences between the cell supernatant and urine in the concentration and proportion of  $EV_{EpCAM-CD9}$ , we optimized the methodology again. Additionally, in the clinical laboratory, it is not suitable to quantify EVs by NTA due to the requirement of

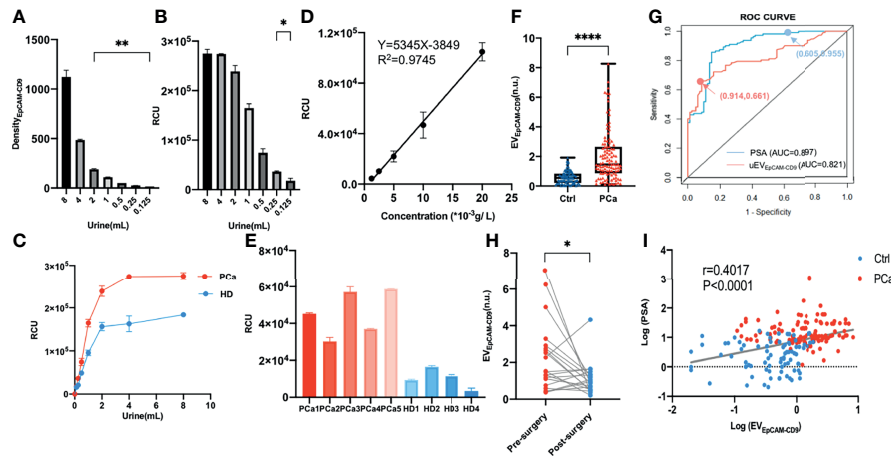


**FIGURE 3** | Urinary EpCAM-CD9-positive EV is a potential biomarker for PCa diagnosis. **(A)** The uEV<sub>EpCAM-CD9</sub> in different urine volumes was detected by WB. **(B)** The uEV<sub>EpCAM-CD9</sub> from different urine volumes was detected by our chemiluminescent immunoassay. **(C)** The uEV<sub>EpCAM-CD9</sub> of the pooled samples from PCa and healthy controls were detected by EV assay. **(D)** A standard curve was for urinary EV quantification using our EV assay. **(E)** The uEV<sub>EpCAM-CD9</sub> from nine randomly selected donors including five PCa and four HDs was assayed by the chemiluminescent immunoassay. **(F)** The levels of uEV<sub>EpCAM-CD9</sub> was observed from men with PCa (n = 112) and without PCa (n = 81). **(G)** The ROC curve of uEV<sub>EpCAM-CD9</sub> and PSA. **(H)** The uEV<sub>EpCAM-CD9</sub> was detected before and after prostatectomy in 20 PCa patients. **(I)** The correlation between the uEV<sub>EpCAM-CD9</sub> and PSA. Density<sub>EpCAM-CD9</sub>, EpCAM-CD9 protein density; RCU, relative chemiluminescent unit; EV<sub>EpCAM-CD9</sub>, EpCAM-CD9-positive extracellular vesicles; Ctrl, control; PCa, prostate cancer; ROC, receiver operating characteristic; uEV<sub>EpCAM-CD9</sub>, urinary EpCAM-CD9-positive extracellular vesicles; PSA, prostate-specific antigen; AUC, area under the curve; HD, healthy donor. \*P < 0.05, \*\*P < 0.01, \*\*\*\*P < 0.0001.

the specialized equipment. And NTA may be biased toward certain particle size ranges (especially 50–150 nm), and large EVs (>400 nm) and very small EVs (<50 nm) are not well quantified by NTA. We thus used a simple and low-cost protein assay, BCA, as an alternative for EV quantification (25). As described in the *Materials and Methods*, we optimized the concentration of CD9 antibody and restructured the standard curve and corresponding performance evaluation. As shown in **Figure 3D**, the RCU value was found to greatly depend on the concentration of EVs, with a good linearity range ranging from  $1.25 \times 10^{-3}$  to  $20.00 \times 10^{-3}$  g/L ( $R^2 = 0.9745$ ) and a low detection limit,  $0.60 \times 10^{-3}$  g/L. The recovery test and repeatability test both performed excellently especially at the low level of uEV<sub>EpCAM-CD9</sub> (**Supplementary Table S2**, right panels). Furthermore, uEV<sub>EpCAM-CD9</sub> from nine randomly selected donors including five PCa and four HDs was assayed by the CLIA and WB, which suggested a significant elevation of uEV<sub>EpCAM-CD9</sub> in PCa compared with HD (**Figure 3E** and **Supplementary Figures S2C, D**).

In the validation experiment, urine samples from a total of 193 participants were further enrolled, including 112 PCa patients, 55 BPH patients, and 26 HDs. Complete datasets were available in 193 men who underwent the first transrectal ultrasound (TRUS)-guided prostate biopsy, and the histologic subtypes of all the 112 PCa patients were identified as prostate adenocarcinoma and without any metastatic sites confirmed by computed tomography examinations. The clinical characteristics of all the participants were listed in **Supplementary Table S1**. A remarkably higher level of uEV<sub>EpCAM-CD9</sub> was observed from men with PCa (1.46, IQR 0.86–2.66) than men without PCa (0.55, IQR 0.22–0.84) (**Figure 3F**). ROC curve showed that the

diagnostic sensitivity and specificity of uEV<sub>EpCAM-CD9</sub> was 66.07% and 91.36%, respectively (cutoff value: 1.130), and the area under the curve (AUC) was 0.821 ( $P < 0.0001$ ), while the diagnostic sensitivity and specificity of PSA was 95.54% and 60.49%, respectively (cutoff value: 4.015), and the AUC was 0.897 ( $P < 0.0001$ ) (**Figure 3G**). Moreover, there was a statistically significant correlation between uEV<sub>EpCAM-CD9</sub> and Gleason grades in PCa patients ( $r = 0.215$ , 95% CI: 0.025–0.389,  $P = 0.023$ ). Significant decreases of uEV<sub>EpCAM-CD9</sub> were observed after prostatectomy in 20 PCa patients (**Figure 3H**). It also showed that uEV<sub>EpCAM-CD9</sub> levels were positively associated with PSA ( $r = 0.402$ , 95% CI: 0.272–0.517,  $P < 0.0001$ ), which was an important indicator for the diagnosis of PCa (**Figure 3I**).

## A Multivariate Diagnostic Model Based on uEV<sub>EpCAM-CD9</sub> for Prostate Cancer

Due to the results that uEV<sub>EpCAM-CD9</sub> has high specificity and low sensitivity, while PSA is just the opposite (**Figure 3G**), we consider building a model combining uEV<sub>EpCAM-CD9</sub> and PSA to better diagnose PCa. The training dataset (n = 116) and validation dataset (n = 77) had an even distribution in patient characteristics (**Table 1**). The predictive value of the uEV<sub>EpCAM-CD9</sub> was analyzed using a logistic regression model. The odds ratio (OR) for each clinical factor and/or covariate in training sets was assessed by univariate logistic regression modeling. Age, uEV<sub>EpCAM-CD9</sub>, PSA, fPSA, f/T PSA, prostate volume (PV), and prostate-specific antigen density (PSAD) were statistically significant predictors of PCa ( $P < 0.001$ ) on univariate logistic regression analysis (**Table 2**, left panels). Then, we compared varieties of multivariate diagnostic models employing different

**TABLE 1** | Baseline characteristics of the training and validation cohorts.

Variable	Training Set (n = 116)			Validation Set (n = 77)		P value
	Men with PCa (n = 69)	Men without PCa (n = 47)	P value	Men with PCa (n = 43)	Men without PCa (n = 34)	
	Median (IQR) or n (%)	Median (IQR) or n (%)		Median (IQR) or n (%)	Median (IQR) or n (%)	
Age (years)	72 (66–76)	64 (51–70)	<0.0001	71 (64–74)	64 (55–73)	0.018
Smoking			0.014			0.127
Yes	30 (43.5)	10 (21.3)		20 (46.5)	10 (29.4)	
No	39 (56.5)	37 (78.7)		23 (53.5)	24 (70.6)	
Drinking			0.026			0.229
Yes	30 (43.5)	11 (23.4)		17 (39.5)	9 (26.5)	
No	39 (56.5)	36 (76.6)		26 (60.5)	25 (73.5)	
Family history			0.167			0.428
Yes	8 (11.6)	2 (4.3)		3 (7.0)	1 (2.9)	
No	61 (88.4)	45 (95.7)		40 (93.0)	33 (97.1)	
BMI (kg/m <sup>2</sup> )	23.88 (22.00–26.03)	22.23 (21.29–24.62)	0.012	23.30 (21.80–25.08)	22.78 (21.72–24.14)	0.538
Gleason score			<0.0001			<0.0001
6	12 (17.4)	NA		5 (11.6)	NA	
7	32 (46.4)	NA		17 (39.5)	NA	
8	12 (17.4)	NA		9 (20.9)	NA	
9–10	13 (18.8)	NA		12 (27.9)	NA	
CEA (ng/ml)	2.6 (2.1–3.5)	2.1 (1.4–3.0)	0.019	2.2 (1.8–3.2)	2.0 (1.5–3.0)	0.228
AFP (ng/ml)	2.6 (1.8–3.5)	2.5 (1.8–3.6)	0.833	2.8 (1.7–3.2)	2.5 (1.6–3.0)	0.285
CA125 (U/ml)	9.9 (7.1–12.8)	11.5 (7.1–13.9)	0.389	11.3 (9.1–14.5)	11.2 (5.5–12.8)	0.327
CA199 (U/ml)	7.4 (4.1–11.3)	7.1 (4.0–11.6)	0.884	6.2 (4.7–11.9)	5.9 (3.7–11.1)	0.432
EpCAM-CD9-positive EV concentration (n.u)	1.38 (0.56–2.48)	0.53 (0.31–0.84)	<0.0001	1.57 (1.15–3.08)	0.58 (0.16–0.91)	<0.0001
PSA (ng/ml)	10.9820 (7.3635–22.0090)	2.6780 (0.8072–5.5960)	<0.0001	14.8340 (9.5180–29.9020)	2.7025 (1.0583–8.3488)	<0.0001
fPSA (ng/ml)	1.5390 (1.0730–3.0710)	0.6777 (0.3045–1.1920)	<0.0001	2.1080 (0.8620–3.2330)	0.7826 (0.2259–1.6068)	<0.0001
f/T PSA	0.13 (0.09–0.20)	0.22 (0.18–0.34)	<0.0001	0.11 (0.08–0.19)	0.23 (0.19–0.29)	<0.0001
PV (cm <sup>3</sup> )	63.00 (44.93–109.35)	66.58 (24.00–107.04)	0.556	54.71 (47.23–77.76)	50.34 (24.00–110.83)	0.785
PSAD (ng/ml <sup>2</sup> )	0.17 (0.08–0.45)	0.04 (0.02–0.06)	<0.0001	0.31 (0.17–0.43)	0.05 (0.03–0.07)	<0.0001

BMI, body mass index; EV, extracellular vesicle; PSA, prostate-specific antigen; fPSA, free prostate-specific antigen; f/T PSA, free/total prostate-specific antigen; PV, prostate volume; PSAD, prostate-specific antigen density; PCa, prostate cancer; IQR, interquartile range; NA, not applicable.

combinations of the variables assessed by their AUC in ROC curve analysis variables (**Supplementary Table S3**). The optimal multivariate model for diagnosing PCa should be selected on the basis of the complexity (numbers of variables) and prediction efficiency (AUC); we rationally selected the multivariate model containing the variable age, smoking, drinking, family history, BMI, uEV<sub>EpCAM-CD9</sub>, PSA, and PV as the final diagnostic model. The OR of each variable from the multivariate logistic regression analysis was presented in **Table 2** (right panels).

The nomogram was constructed according to the results of multivariate logistic regression (**Figure 4A**). In the ROC curve analysis, the AUC of the combined PCa diagnostic model was increased to 0.952 in the training set (**Figure 4B**). Moreover, the multivariate diagnostic model was perfectly in the internal validations, as the calibration curve showed good agreement between prediction and observation (**Figure 4C**). On DCA, by combining uEV<sub>EpCAM-CD9</sub> with other clinical parameters, the combination model to predict PCa added more clinical overall benefit than that of uEV<sub>EpCAM-CD9</sub> only (**Figure 4D**). When applied to the validation test, the model achieved an AUC of 0.947 ( $P < 0.0001$ ) (**Figure 4B**). The AUC value revealed the high performance of PCa diagnosis using the combined nomogram.

Additionally, in patients with PSA gray zone (4–10 ng/ml) including 23 PCa and 31 BPH, the model based on uEV<sub>EpCAM-CD9</sub> showed a better diagnostic performance (AUC = 0.917,  $P < 0.0001$ ) than the uEV<sub>EpCAM-CD9</sub> only (AUC = 0.887,  $P < 0.0001$ ) and the traditional biomarkers PSA (AUC = 0.712,  $P = 0.0018$ ) (**Figure 4E**).

## DISCUSSION

EVs represent a rich source of information in many liquid biopsy samples, including plasma, serum, and urine, since they are abundantly released by most tumors and are relatively stable in the biological fluids, whereas cell-free nucleic acids suffer rapid degradation and are always presented at low concentration (26). PCa cell-derived EVs in urine have been extensively studied recently and regarded as novel biomarkers for cancer diagnosis. However, the major concern about the use of EVs as biomarkers in the clinical laboratory is the difficulties in the characterization of EVs. Consequently, there will be essential interest in developing standardized sampling and analytical techniques for reliable and reproducible measurements. CLIA is



**TABLE 2 |** Univariate analysis and multivariate analysis of potential predictors of PCa.

Variable	Univariate analysis		Multivariate analysis	
	OR (95% CI)	P value	OR (95% CI)	P value
Age (years)	1.090 (1.053–1.129)	<0.001	1.019 (0.962–1.080)	0.515
Smoking	2.460 (1.313–4.607)	0.005	0.579 (0.148–2.268)	0.433
Drinking	2.205 (1.176–4.138)	0.014	1.690 (0.462–6.178)	0.428
Family history	2.832 (0.764–10.498)	0.119	4.386 (0.452–42.528)	0.202
BMI ( $\geq 24$ kg/m <sup>2</sup> vs. <24 kg/m <sup>2</sup> )	2.186 (1.188–4.019)	0.012	1.312 (0.433–3.976)	0.631
CEA (ng/ml)	1.227 (0.988–1.523)	0.064		
AFP (ng/ml)	1.109 (0.937–1.313)	0.228		
CA125 (U/ml)	1.016 (0.965–1.069)	0.545		
CA199 (U/ml)	1.002 (0.980–1.025)	0.836		
Log EpCAM-CD9-positive EV concentration (n.u)	15.392 (6.377–37.149)	<0.001	28.745 (6.438–128.346)	<0.001
PSA (ng/ml)				
<4	Reference	<0.001	Reference	<0.001
4–10	15.200 (5.301–43.581)	<0.001	33.292 (6.105–181.543)	<0.001
>10	73.600 (23.220–233.284)	<0.001	169.450 (25.652–1119.355)	<0.001
fPSA (ng/ml)	2.007 (1.470–2.742)	<0.001		
f/T PSA	0.000 (0.000–0.003)	<0.001		
PV (cm <sup>3</sup> )				
<36	Reference	<0.001	Reference	0.001
36–48	6.462 (2.079–20.086)	0.001	1.384 (0.173–11.083)	0.760
48–72	9.333 (2.079–24.838)	<0.001	3.352 (0.489–22.973)	0.218
72–108	2.741 (0.981–7.661)	0.054	0.203 (0.025–1.636)	0.134
>108	2.234 (0.961–5.194)	0.062	0.088 (0.012–0.633)	0.016
PSAD ( $\geq 0.15$ ng/ml <sup>2</sup> vs. <0.15 ng/ml <sup>2</sup> )	68.402 (15.964–293.082)	<0.001		

PCa, prostate cancer; BMI, body mass index; EV, extracellular vesicle; PSA, prostate-specific antigen; fPSA, free prostate-specific antigen; f/T PSA, free/total prostate-specific antigen; PV, prostate volume; PSAD, prostate-specific antigen density; OR, odds ratio; CI, confidence interval.

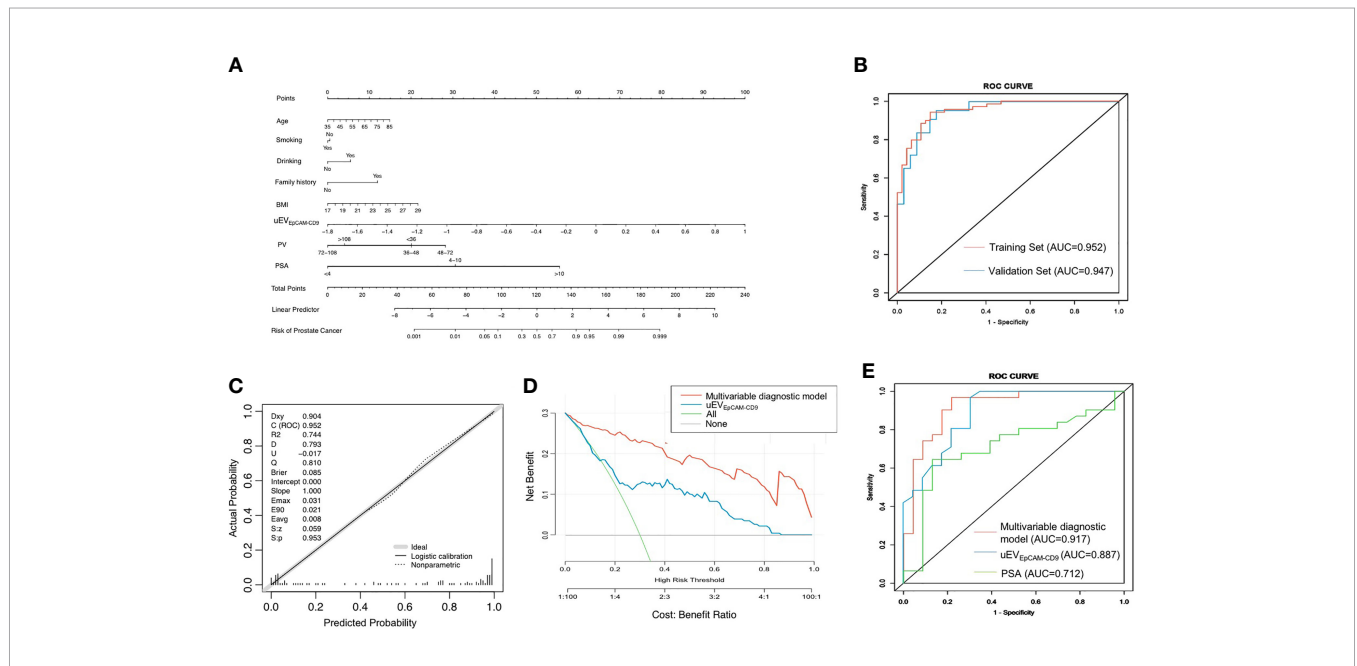


**FIGURE 4 |** A multivariate diagnostic model based on uEV<sub>EpCAM-CD9</sub> for PCa. **(A)** The nomogram was constructed according to the results of multivariate logistic regression. **(B)** The ROC curve analysis of the multivariable diagnostic model in the training set and validation set. **(C)** The multivariable diagnostic model was calibrated in the internal validations. **(D)** The decision curve analysis of the multivariable diagnostic model and uEV<sub>EpCAM-CD9</sub>. **(E)** The diagnostic performance of the model, uEV<sub>EpCAM-CD9</sub>, and PSA in patients with PSA gray zone (4–10 ng/ml) including 23 PCa and 31 BPH. BMI, body mass index; uEV<sub>EpCAM-CD9</sub>, Log urinary EpCAM-CD9-positive extracellular vesicles concentration (n.u); PV, prostate volume; PSA, prostate-specific antigen; ROC, receiver operating characteristic; AUC, area under the curve.

a non-isotopic immunological technique that is increasingly used in ultramicroanalysis of biological substances owing to extreme sensitivity, high specificity, good reproducibility, and simplicity (27, 28). In this study, we proposed a chemiluminescent quantitative immunoassay of uEV<sub>EpCAM-CD9</sub>, requiring only a small volume of urine (125  $\mu$ l) to perform an EV analysis, which is superior to WB and flow cytometry (29). The extremely low LOD of EpCAM revealed that it was possible to detect other non-abundant proteins on EVs by employing multiple antibody sets. Furthermore, the use of CLIA embodies the superiority that could be fully automated to reduce operator errors and bias and enhance its potential for clinical translation.

EpCAM (also known as CD326) is deemed as a cancer-associated marker, as it is always overexpressed in many human adenocarcinomas and squamous cell carcinomas (30). Besides, this expression often closely correlates with the epithelial-mesenchymal transition (EMT)-regulating tumor invasion and metastasis (31, 32): the tumor cells have been observed to undergo loss of EpCAM expression during EMT and release a large number of EpCAM-enriched EVs simultaneously (32, 33). The source and the underlying functions of these EVs in PCa, however, remain unknown. It has been suggested that the cancerous cells will proliferate more rapidly due to the dysregulated cell cycle resulting in a state of oxygen and nutrient deprivation, and adaptation to such microenvironments is pivotal to tumor growth (34). There is good evidence that many signaling pathways are involved to help the cells escape from stresses such as hypoxia and nutrient deprivation and determine cell growth, promotion, metastasis, hormone-refractory progression, and treatment outcome (35, 36). Additionally, previous studies have reported that higher numbers of EVs were secreted by cancer cells to offer a survival advantage to cells and promote cancer progression under hypoxia and serum starvation (37, 38). These EVs usually promoted the PCa aggressiveness by adhesion junction proteins that could enhance invasiveness and induce microenvironment changes (39). Thus, such mechanisms may account for the elevated levels of PCa cell-derived EV<sub>EpCAM-CD9</sub> under simulated tumor microenvironment (such as hypoxia and serum starvation), as well as in PCa patients.

However, uEV<sub>EpCAM-CD9</sub> was not prostate-specific; that is, it may be over-released by other urogenital tumors such as bladder and kidney and other non-urogenital cancers. Recalling that the levels are commonly very low in HDs and patients with BPH, our multivariate model employing uEV<sub>EpCAM-CD9</sub>, prostate tissue-specific protein (PSA), and other clinical parameters showed an enhanced diagnostic performance both in sensitivity and specificity. We also envision that by combining other cancer biomarkers, such as metabolites, RNAs or genetic signatures and medical imaging data could further provide more precise information regarding PCa diagnosis and localization.

Another limitation is the number of samples studied ( $n = 193$ ). We only evaluated the diagnostic value of uEV<sub>EpCAM-CD9</sub> in PCa, and it has not been evaluated in depth in other aspects, e.g., as a predictor in the development of castration-resistant prostate cancer (CRPC), an indicator for successful radiotherapy and chemotherapy. Besides, while EV<sub>EpCAM-CD9</sub> can be released from different types of epithelial cancers and the diagnostic

performance of uEV<sub>EpCAM-CD9</sub> in these cancers remains poorly investigated, further large-scale studies will be warranted to fully evaluate the potential applications of uEV<sub>EpCAM-CD9</sub> with regard to the diagnosis of varieties of cancers.

## CONCLUSIONS

Urinary EpCAM-CD9-positive EVs were successfully quantified by our laboratory-developed CLIA, requiring only a small volume of urine (125  $\mu$ l) to perform an EV analysis. Using this assay, we achieve a notable diagnostic performance by constructing a multivariate diagnostic model based on uEV<sub>EpCAM-CD9</sub> and a tissue-specific biomarker PSA. Further validation studies are warranted and should also investigate before its clinical value can be confidently affirmed. In the future, this model may potentially be used to better select patients for prostate TRUS biopsy.

## DATA AVAILABILITY STATEMENT

The raw data supporting the conclusions of this article will be made available by the authors without undue reservation.

## ETHICS STATEMENT

The studies involving human participants were reviewed and approved by the Second Affiliated Hospital of Zhejiang University School of Medicine Ethical Committee. The patients/participants provided their written informed consent to participate in this study.

## AUTHOR CONTRIBUTIONS

YD, YW, XW, and ZT planned the project, performed the research, analyzed the data, and wrote the article. YC, YS, and DW collected clinical samples. PY and LZ performed statistical analysis. ZL, YP, and GZ collected patient information and analyzed the data. All authors contributed to the article and approved the submitted version.

## FUNDING

This study was supported by grants from the National Natural Science Foundation of China Youth Science Foundation Project (Grant no. 81902156) and Zhejiang Provincial Natural Science Foundation of China (Grant no. LQ21H160016).

## SUPPLEMENTARY MATERIAL

The Supplementary Material for this article can be found online at: <https://www.frontiersin.org/articles/10.3389/fonc.2021.777684/full#supplementary-material>

## REFERENCES

- Sung H, Ferlay J, Siegel RL, Laversanne M, Soerjomataram I, Jemal A, et al. Global Cancer Statistics 2020: GLOBOCAN Estimates of Incidence and Mortality Worldwide for 36 Cancers in 185 Countries. *CA Cancer J Clin* (2021) 71:209–49. doi: 10.3322/caac.21660
- Martin R, Donovan J, Turner E, Metcalfe C, Young G, Walsh E, et al. Effect of a Low-Intensity PSA-Based Screening Intervention on Prostate Cancer Mortality: The CAP Randomized Clinical Trial. *JAMA* (2018) 319:883–95. doi: 10.1001/jama.2018.0154
- Brassell SA, Kao TC, Sun L, Moul JW. Prostate-Specific Antigen Versus Prostate-Specific Antigen Density as Predictor of Tumor Volume, Margin Status, Pathologic Stage, and Biochemical Recurrence of Prostate Cancer. *Urology* (2005) 66:1229–33. doi: 10.1016/j.urolgy.2005.06.106
- Sanda M, Feng Z, Howard D, Tomlins S, Sokoll L, Chan D, et al. Association Between Combined TMPRSS2:ERG and PCA3 RNA Urinary Testing and Detection of Aggressive Prostate Cancer. *JAMA Oncol* (2017) 3:1085–93. doi: 10.1001/jamaoncol.2017.0177
- Crawford E, Rove K, Trabulsi E, Qian J, Drownowska K, Kaminetsky J, et al. Diagnostic Performance of PCA3 to Detect Prostate Cancer in Men With Increased Prostate Specific Antigen: A Prospective Study of 1,962 Cases. *J Urol* (2012) 188:1726–31. doi: 10.1016/j.juro.2012.07.023
- Laxman B, Tomlins S, Mehra R, Morris D, Wang L, Helgeson B, et al. Noninvasive Detection of TMPRSS2:ERG Fusion Transcripts in the Urine of Men With Prostate Cancer. *Neoplasia (New York NY)* (2006) 8:885–8. doi: 10.1593/neo.06625
- Van Neste L, Partin A, Stewart G, Epstein J, Harrison D, Van Criekinge W. Risk Score Predicts High-Grade Prostate Cancer in DNA-Methylation Positive, Histopathologically Negative Biopsies. *Prostate* (2016) 76:1078–87. doi: 10.1002/pros.23191
- Davey M, Benzina S, Savoie M, Breault G, Ghosh A, Ouellette R. Affinity Captured Urinary Extracellular Vesicles Provide mRNA and miRNA Biomarkers for Improved Accuracy of Prostate Cancer Detection: A Pilot Study. *Int J Mol Sci* (2020) 21:8330. doi: 10.3390/ijms21218330
- Kohaar I, Chen Y, Banerjee S, Borbiev T, Kuo H, Ali A, et al. A Urine Exosome Gene Expression Panel Distinguishes Between Indolent and Aggressive Prostate Cancers at Biopsy. *J Urol* (2021) 205:420–5. doi: 10.1097/ju.0000000000001374
- Merchant M, Rood I, Deegens J, Klein J. Isolation and Characterization of Urinary Extracellular Vesicles: Implications for Biomarker Discovery. *Nat Rev Nephrol* (2017) 13:731–49. doi: 10.1038/nrneph.2017.148
- Pisitkun T, Shen R, Knepper M. Identification and Proteomic Profiling of Exosomes in Human Urine. *Proc Natl Acad Sci USA* (2004) 101:13368–73. doi: 10.1073/pnas.0403453101
- Gonzales P, Pisitkun T, Hoffert J, Tchapyjnikov D, Star R, Kleta R, et al. Large-Scale Proteomics and Phosphoproteomics of Urinary Exosomes. *J Am Soc Nephrol: JASN* (2009) 20:363–79. doi: 10.1681/asn.2008040406
- Moon P, You S, Lee J, Hwang D, Baek M. Urinary Exosomes and Proteomics. *Mass Spectrometry Rev* (2011) 30:1185–202. doi: 10.1002/mas.20319
- Gires O, Pan M, Schinke H, Canis M, Baeuerle P. Expression and Function of Epithelial Cell Adhesion Molecule EpCAM: Where Are We After 40 Years? *Cancer Metastasis Rev* (2020) 39:969–87. doi: 10.1007/s10555-020-09898-3
- Fagotto F, Aslemar A. EpCAM Cellular Functions in Adhesion and Migration, and Potential Impact on Invasion: A Critical Review. *Biochim Biophys Acta Rev Cancer* (2020) 1874:188436. doi: 10.1016/j.bbcan.2020.188436
- Miller M, Doyle G, Terstappen L. Significance of Circulating Tumor Cells Detected by the CellSearch System in Patients With Metastatic Breast Colorectal and Prostate Cancer. *J Oncol* (2010) 2010:617421. doi: 10.1155/2010/617421
- Pu K, Li C, Zhang N, Wang H, Shen W, Zhu Y. Epithelial Cell Adhesion Molecule Independent Capture of Non-Small Lung Carcinoma Cells With Peptide Modified Microfluidic Chip. *Biosensors Bioelectron* (2017) 89:927–31. doi: 10.1016/j.bios.2016.09.092
- Wei P, Wu F, Kang B, Sun X, Heskia F, Pachot A, et al. Plasma Extracellular Vesicles Detected by Single Molecule Array Technology as a Liquid Biopsy for Colorectal Cancer. *J Extracell Vesicles* (2020) 9:1809765. doi: 10.1080/20013078.2020.1809765
- Sunkara V, Kim C, Park J, Woo H, Kim D, Ha H, et al. Fully Automated, Label-Free Isolation of Extracellular Vesicles From Whole Blood for Cancer Diagnosis and Monitoring. *Theranostics* (2019) 9:1851–63. doi: 10.7150/thno.32438
- Théry C, Witwer K, Aikawa E, Alcaraz M, Anderson J, Andriantsitohaina R, et al. Minimal Information for Studies of Extracellular Vesicles 2018 (MISEV2018): A Position Statement of the International Society for Extracellular Vesicles and Update of the MISEV2014 Guidelines. *J Extracell Vesicles* (2018) 7:1535750. doi: 10.1080/20013078.2018.1535750
- Wang Y, Liu Z, Wang X, Dai Y, Li X, Gao S, et al. Rapid and Quantitative Analysis of Exosomes by a Chemiluminescence Immunoassay Using Superparamagnetic Iron Oxide Particles. *J BioMed Nanotechnol* (2019) 15:1792–800. doi: 10.1166/jbn.2019.2809
- Osteikoetxea X, Sódar B, Németh A, Szabó-Taylor K, Pálóczi K, Vukman K, et al. Differential Detergent Sensitivity of Extracellular Vesicle Subpopulations. *Organic Biomol Chem* (2015) 13:9775–82. doi: 10.1039/c5ob01451d
- Han L, Lam E, Sun Y. Extracellular Vesicles in the Tumor Microenvironment: Old Stories, But New Tales. *Mol Cancer* (2019) 18:59. doi: 10.1186/s12943-019-0980-8
- Maacha S, Bhat A, Jimenez L, Raza A, Haris M, Uddin S, et al. Extracellular Vesicles-Mediated Intercellular Communication: Roles in the Tumor Microenvironment and Anti-Cancer Drug Resistance. *Mol Cancer* (2019) 18:55. doi: 10.1186/s12943-019-0965-7
- Lötvall J, Hill A, Hochberg F, Buzás E, Di Vizio D, Gardiner C, et al. Minimal Experimental Requirements for Definition of Extracellular Vesicles and Their Functions: A Position Statement From the International Society for Extracellular Vesicles. *J Extracell Vesicles* (2014) 3:26913. doi: 10.3402/jev.v3.26913
- Neumann M, Bender S, Krahn T, Schlange T. ctDNA and CTCs in Liquid Biopsy - Current Status and Where We Need to Progress. *Comput Struct Biotechnol J* (2018) 16:190–5. doi: 10.1016/j.csbj.2018.05.002
- Zhao L, Sun L, Chu X. Chemiluminescence Immunoassay. *TrAC Trends Anal Chem* (2009) 28:404–15. doi: 10.1016/j.trac.2008.12.006
- Akhavan-Tafti H, Binger DG, Blackwood JJ, Chen Y, Creager RS, de Silva R, et al. A Homogeneous Chemiluminescent Immunoassay Method. *J Am Chem Soc* (2013) 135:4191–4. doi: 10.1021/ja312039k
- Campos-Silva C, Suárez H, Jara-Acevedo R, Linares-Espinós E, Martínez-Piñero L, Yáñez-Mó M, et al. High Sensitivity Detection of Extracellular Vesicles Immune-Captured From Urine by Conventional Flow Cytometry. *Sci Rep* (2019) 9:2042. doi: 10.1038/s41598-019-38516-8
- Went P, Lugli A, Meier S, Bundi M, Mirlacher M, Sauter G, et al. Frequent EpCAM Protein Expression in Human Carcinomas. *Hum Pathol* (2004) 35:122–8. doi: 10.1016/j.humpath.2003.08.026
- Sankpal NV, Fleming TP, Sharma PK, Wiedner HJ, Gillanders WE. A Double-Negative Feedback Loop Between EpCAM and ERK Contributes to the Regulation of Epithelial-Mesenchymal Transition in Cancer. *Oncogene* (2017) 36:3706–17. doi: 10.1038/onc.2016.504
- Gao J, Yan Q, Wang J, Liu S, Yang X. Epithelial-To-Mesenchymal Transition Induced by TGF-β1 Is Mediated by AP1-Dependent EpCAM Expression in MCF-7 Cells. *J Cell Physiol* (2015) 230:775–82. doi: 10.1002/jcp.24802
- Ye X, Tam W, Shibue T, Kaygusuz Y, Reinhardt F, Ng Eaton E, et al. Distinct EMT Programs Control Normal Mammary Stem Cells and Tumour-Initiating Cells. *Nature* (2015) 525:256–60. doi: 10.1038/nature14897
- Kalaany N, Sabatini D. Tumours With PI3K Activation Are Resistant to Dietary Restriction. *Nature* (2009) 458:725–31. doi: 10.1038/nature07782
- Fraga A, Ribeiro R, Principe P, Lopes C, Medeiros R. Hypoxia and Prostate Cancer Aggressiveness: A Tale With Many Endings. *Clin Genitourin Cancer* (2015) 13:295–301. doi: 10.1016/j.clgc.2015.03.006
- Li X, Lao Y, Zhang H, Wang X, Tan H, Lin Z, et al. The Natural Compound Guttiferone F Sensitizes Prostate Cancer to Starvation Induced Apoptosis via Calcium and JNK Elevation. *BMC Cancer* (2015) 15:254. doi: 10.1186/s12885-015-1292-z
- Panigrahi GK, Praharaj PP, Peak TC, Long J, Singh R, Rhim JS, et al. Hypoxia-Induced Exosome Secretion Promotes Survival of African-American and Caucasian Prostate Cancer Cells. *Sci Rep* (2018) 8:3853. doi: 10.1038/s41598-018-22068-4
- Umezumi T, Tadokoro H, Azuma K, Yoshizawa S, Ohyashiki K, Ohyashiki J. Exosomal miR-135b Shed From Hypoxic Multiple Myeloma Cells Enhances Angiogenesis by Targeting Factor-Inhibiting HIF-1. *Blood* (2014) 124:3748–57. doi: 10.1182/blood-2014-05-576116

39. Ramteke A, Ting H, Agarwal C, Mateen S, Somasagara R, Hussain A, et al. Exosomes Secreted Under Hypoxia Enhance Invasiveness and Stemness of Prostate Cancer Cells by Targeting Adherens Junction Molecules. *Mol Carcinog* (2015) 54:554–65. doi: 10.1002/mc.22124

**Conflict of Interest:** The authors declare that the research was conducted in the absence of any commercial or financial relationships that could be construed as a potential conflict of interest.

**Publisher's Note:** All claims expressed in this article are solely those of the authors and do not necessarily represent those of their affiliated organizations, or those of

the publisher, the editors and the reviewers. Any product that may be evaluated in this article, or claim that may be made by its manufacturer, is not guaranteed or endorsed by the publisher.

*Copyright © 2021 Dai, Wang, Cao, Yu, Zhang, Liu, Ping, Wang, Zhang, Sang, Wang and Tao. This is an open-access article distributed under the terms of the Creative Commons Attribution License (CC BY). The use, distribution or reproduction in other forums is permitted, provided the original author(s) and the copyright owner(s) are credited and that the original publication in this journal is cited, in accordance with accepted academic practice. No use, distribution or reproduction is permitted which does not comply with these terms.*